Study of the extinction law in M 31 and selection of red supergiants

Petko Nedialkov[1], Todor Veltchev[1]
Department of Astronomy, University of Sofia,
5 James Bourchier Blvd., Sofia 1164, Bulgaria
japet@phys.uni-sofia.bg, eirene@phys.uni-sofia.bg
(Submitted on 06.01.2015; Accepted on 22.01.2015)

Abstract. An average value of the total-to-selective-extinction ratio $R_V = 3.8 \pm 0.4$ in M 31 is obtained by means of two independent methods and by use of the analytical formula of Cardelli, Clayton & Mathis (1989). This result differs from previous determinations as well from the 'standard' value 3.1 for the Milky Way. The derived individual extinctions for blue and red luminous stars from the catalogue of Magnier et al. (1992) are in good agreement with recent estimates for several OB associations in M 31 and thus the issue about the assumed optical opacity of the spiral disk still remains open.
The presented list of 113 red supergiant candidates in M 31 with their extinctions and luminosities contains 60 new objects of this type which are not identified in other publications. It is supplemented with further 290 stars dereddened on the base of results for their closest neighbors. The luminosity function of all red supergiant candidates and the percentage of those with progenitors over 20 $M_\odot$ suggests that the evolution of massive stars in M 31 resembles that in other Local Group galaxies.
Key words: interstellar medium: extinction – galaxies: individual (M 31) – stars: redeening – stars: red supergiants

Introduction

The interstellar dust affects considerably the statistics and the magnitudes of the brightest stars in nearby galaxies. Its physical properties influence the extinction law $A(\lambda)/A(V)$ or $E(\lambda - V)/E(B - V)$ which is recently – in most of these systems – still poorly known due to insufficient data. The observational derivation of this law is possible by determination of the total-to-selective-extinction ratio $R_V = A(V)/E(B - V)$ or of the reddening line slopes in the colour-colour diagrams. Shortly before his depart Baade said (as quoted by van den Bergh 1968) if he is allowed to choose again, he would become an astronomer only on condition that R_V is everywhere constant. There exist nowadays undoubted indications that the average extinction law in our Galaxy depending solely on R_V is applicable both to the diffuse and the dense regions of the interstellar medium (Cardelli, Clayton & Mathis 1989; hereafter CCM). Unfortunately the large distances and the faint fluxes restrict the spectroscopic studies in external galaxies – and hence the study of R_V – to observations of high-luminosity stars.

The Andromeda galaxy M 31 is a favoured object for comparative investigations and in the last years appeared new results about the extinction in it. Combining CCD photometry and spectroscopic data for hot luminous stars, Massey et al. (1995) (hereafter MAP95) obtained an average slope of the reddening line $E(U - B)/E(B - V) = 0.5 \pm 0.07$ which is quite different from the 'normal' value of 0.7 in the Milky Way. Bianchi et al. (1996) derived an ultraviolet extinction curve resembling that of the Galaxy with possible weakness (significance of 1σ) at the 2175 Å bump. In view of these ambiguous results the knowledge of R_V in M 31 toward lines of sight with higher reddening is recently of great significance since:

1. This parameter determines the absorption corrections of the stellar magnitude, which are crucial for clarifying the evolutionary status of the brightest stars in M 31, and it gives clue to distinguish them from the foreground dwarfs (see the review in Massey 1998 /hereafter PM98/ and the references therein).

2. It plays an important role in the transformation chain: colour excess E(B-V) $\rightarrow$ extinction $A_V \rightarrow$ optical thickness τ, and thus it contributes to the study of disk's opacity.

The high average metallicity Z in M 31 is a well known fact (Zaritsky, Kennicutt Jr. & Huchra 1994). According to the recent theory of massive stars' evolution the mass-loss rate through stellar winds increases critically with Z (Kudritzki et al. 1989) which should lead to lowering of the upper mass limit of the red supergiants (RSGs) (see Chiosi & Maeder 1986). In PM98 this prediction was supported with two facts pointed out: the lack of confirmed RSGs of higher mass and luminosity in M 31 and the metallicity-dependant red shift of their true colours in comparison with other Local Group galaxies. These results, however, allow an alternative explanation: a higher mean extinction due to large amount of dust would cause poorer statistics of the considered stars while the mentioned red shift may indicate insufficient dereddening. The optical depth of the spiral disks is assumed to correlate with the morphological type of the galaxy and its mean surface brightness (Valentijn 1994). Thus the disk of M 31 (Sb type) would contain much more dust and should be less transparent in comparison with other Local Group systems studied by PM98. One need to mention also the limited statistics of Massey's data – restricted to several OB associations – in view of the angular size of M 31 (4×1.5 deg at the isophote $26^m/\mathrm{arcsec}^2$ in B-passband). For an extensive survey of RSGs should be used an exclusive catalogue which covers the entire galaxy and contains photometry in passbands of longer effective wavelengths. Such requirements meets the $BVRI$ catalogue of Magnier et al. (1992) (hereafter MLV) supplemented later by Haiman et al. (1994a).

The main goal of our work was to derive the extinction law in M 31 as a first step to obtaining a detailed absorption map of the galaxy. In the course of this work we selected a considerable number of red stars that with high probability do not belong to the foreground and therefore are RSG candidates. In Section 2 we review the used observational data of MLV and discuss the issue of the blended images. Section 3 is dedicated to the exact determination of the parameter R_V as the efficiency of two alternative approaches is critically examined. In Section 4 we present the results of dereddening for two samples blue and red stars as well the distribution of the total extinctions with M_V. The list of the selected RSG candidates is considered in Section 5 with reference to the studies of Humphreys et al. (1988) and PM98. Its completeness and luminosity function are discussed in Section 6. Section 7 contains a short summary of the main results.

1. Observational data and their reduction

1.1. The samples and the contamination of foreground Stars

Our study of the extinction in M 31 is based on the large catalogue with $BVRI$ CCD photometry of MLV and its extension by Haiman et al. (1994a). On the base of these data Haiman et al. (1994b) obtained extinction estimates for 11 associations and 9 groups of associations in the eastern and western spiral arms. The electronic version of the catalogue contains 485,388 objects classified in each filter by DoPHOT procedure (Schechter, Mateo & Saha 1993) according to the characteristics of their profile. In view of our task to perform correct dereddening in colour-colour diagrams we composed two samples with BVI and with VRI photometry and one larger sample with VI photometry for selecting a larger list of RSG candidates. Preliminary restriction of the number of blended images and nonstellar objects was achieved with the requirement each image to be classified as a star in at least one filter and to have neither extended nor double profile in the other two. This procedure does not solve completely the problem with blending to which we turn again in the next subsection.

The contamination from Galactic dwarfs may play significant role in samples of stars supposed to belong to large-angular-size extragalactic objects. Predictions about the percentage of foreground stars for given bin size in colour-colour and colour-magnitude diagrams could be made on the base of extensive models of the Milky Way. Such a model was recently developed at the Observatory of Besancon, France (Robin 1994). It is available in electronic form and gives opportunity for fine tuning of magnitude, colour bin sizes and other parameters (photometric errors, angular size of the object etc.), unlike the traditionally used model of Ratnatunga & Bahcall (1985). The simulations' outcome turned out to be sensitive to the adopted fits of photometric errors σ_B and σ_V as functions of magnitude. Therefore we optimized gradually our fits testing at each step the predicted numbers in different bins of diagram V vs. $(B-V)$ with the real counts of foreground stars in a nearby field of M 31 (Berkhuijsen et al. 1988). Reaching satisfactory agreement, we obtained model results for diagrams $(B-V)$ vs. $(V-I)$ and V vs. $(V-I)$ where we plotted the stars from our samples. About 5% of the subsample of 1231 blue stars selected for dereddening in colour-colour diagram could be dwarfs from our Galaxy (see Section 4 for details). The requirements for building a list of RSG candidates with VRI photometry and dereddened colours practically exclude the foreground stars. The group of RSG candidates with VI photometry suffers probably from more significant contamination in the ranges $V < 18.$, $2.0 < (V-I) < 2.2$.

Identifying all of the red stars in our samples with the lists of PM98, we found a systematic difference in V as illustrated in Figure 1 (left). There are serious reasons to believe that the photometry of Massey is more accurate. His observations were obtained with the 2.1 m Kitt Peak telescope and their resolution is, of course, better than that of MLV. On the other side, the V magnitudes in PM98 are in excellent agreement with the Hubble-Space-Telescope (HST) photometry of Hunter et al. (1996) (hereafter HBOL) whereas the values of MLV are obviously lower than the real ones (see Table 1). The latter effect may be recognized also in diagram $(V-R)$ vs. $(V-I)$

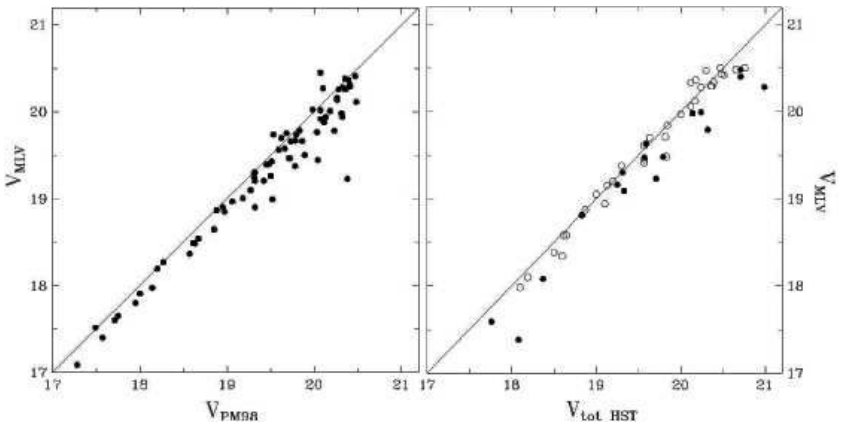

Fig. 1. Comparison of the MLV photometry of red stars (Y axis) with two more recent works on M31: (left) PM98; (right) HBOL (there $V_{\mathrm{tot,\,HST}}$ denotes the integral magnitude of the components to which a 'star' from the MLV catalogue is resolved and the identified blue stars are also plotted (open circles).

where the narrow area with highest density of red stars turned out to be parallely shifted from the zero-absorption line toward 'negative excesses'. Therefore we added to the V magnitudes of our red stars a constant correction $\Delta_V = 0.22$ – an averaged value derived from the less-squares fit for the points in Figure 1 (left).

Table 1. Singular red images from MLV and their identification in PM98 and HBOL. The subscripts indexes denote the work of reference. Columns 4 to 6 contain some notes from PM98: is the star isolated (I) or it is situated in a crowded field (C); which is its spectral class (Sp) (if determined); is it classified as a RSG (rsg) or as a foreground dwarf (fgd).

$\#_{\mathrm{MLV}}$	$\#_{\mathrm{PM98}}$	$\#_{\mathrm{HBOL}}$	I/C	Sp	R/F	V_{MLV}	V_{PM98}	V_{HBOL}	I_{MLV}	I_{HBOL}
95602	78243	300048	I		rsg	19.73	20.05	20.11	17.78	17.79
95879	78819	400011	C	K7I:	rsg	19.42	19.61	19.66	17.65	17.71
96624	781114	300043	C		rsg	19.82	20.23	20.01	17.41	17.05
99714	78588	300029	I		fgd	19.48	19.72	19.79	17.46	17.82
98242	78196	300034	C	M1:I:	rsg	19.70	19.62	19.85	17.22	17.47
98447	78728	300030	C		rsg	19.75	19.68	19.79	17.57	17.65
103801	78705	200020	C		rsg	19.83	19.51	19.55	17.82	17.09
105354	78191	200055	I		rsg	20.04	20.23	20.35	17.76	17.48
95473	78538	400016	C	M0I	rsg	18.72	19.11	19.92	16.50	16.63

1.2. The problem of blended images

Certainly, any ground-based stellar photometry in the field of M 31 obtained with a telescope of moderate resolution could be influenced by se-

vere blending in the crowded regions of OB associations. HBOL warn for this effect and illustrate it with a single example: within radius of 1 arcsec HST detected 26 stars with total magnitude close to an earlier estimate for individual 'stellar' object but the brightest component was 2^m fainter. Comparing high-resolution HST data and images obtained with 1.2 and 1.3 m telescopes, Mochejska et al. (2000) found significant contributions of unresolved luminous companions (19% on the average) to the measured fluxes of the Cepheids. Since MLV performed their observations with one of those telescopes one should expect that their catalogue is also seriously affected by blending. Judging from the left cutoff of the FWHM's distribution (see Figure 2 in MLV), that effect takes place for sizes well below 2.5 arcsec and all multiple groups below 1.5 arcsec are unresolved.

Haiman et al. (1994b) pointed out blending and differential reddening as possible reasons for widening of the Main sequence in colour-magnitude diagrams but, interestingly, they failed to explain with blending the considerable spread of the stellar objects in colour-colour diagrams. Finding the MLV data not accurate enough and perhaps assuming a lot of photometric errors, they give up to use the Q-method and derive the extinction values after study of the colour-magnitude diagrams for the eleven richest associations. The noticeable number of stars with positions in colour-colour diagram over the reddening vector for the bluest spectral type O5 was interpreted with variety of extinction laws (different R_V's). That is the case even with OB 78 – the positions of many objects correspond to $R_V > 6.3$ (see Figure 8 in Haiman et al. 1994b; there OB 013=OB 78) whereas the recent study of Veltchev, Nedialkov & Ivanov (1999) reveals small gas density and vanishing internal extinction probably due to exhaustion of the natal cloud material.

OB 78 (NGC 206) contains numerous well crowded stars of high luminosity. Thus the HST photometry of HBOL for this giant complex, juxtaposed with the work of MLV, allows us to check the effect of blending in our extinction determinations. The identification level of objects brighter than $V = 20.5$ turned out to be close to 100%. The analysis shows that 49 from 100 identified stars over the completeness limit are substantially blended within radius of 1.5 arcsec. This size is slightly higher than 1/2 of the typical FWHM value in the data used (2.5 arcsec) and accounts also for possible errors in determining positions of the image centers.

In Figure 1 (right) we compare the MLV magnitudes of blue and red blended objects with the integral magnitudes of the components to which they are resolved in the HST. The picture confirms the already discussed systematic difference in V band of the MLV red stars' photometry and thus justifies the correction we added to it. Considering the resolved groups in which the brightest component dominates noticeably, we found that in 40% of the cases it is a single OB star while a RSG dominates twice rarely. There are configurations of one bright blue and one bright red component (20% of the cases) as well more complicated mixtures. Eventually, the effect of blending produces predominantly objects of intermediate colour. That's why one finds in diagram V vs. $(V - I)$ of MLV a considerable amount of yellow stars whereas in reality, as it is seen in Figure 4a of HBOL, in NGC 206 only a few exist.

The effect of blending becomes even more obvious in the colour-colour

diagram where the MLV photometry in B band has to be added. From Figure 2 it is clear that clouds of blended images cover mainly areas over the reddening line for spectral type O5 and with 'normal' slope. Thereby larger values of R_V are simulated. One possible way to diminish the percentage of blended images is to use a reddening line which demarcates the large dense cloud of blended images from area where singular images dominate. This approach was applied as a part of our dereddening procedure for blue stars.

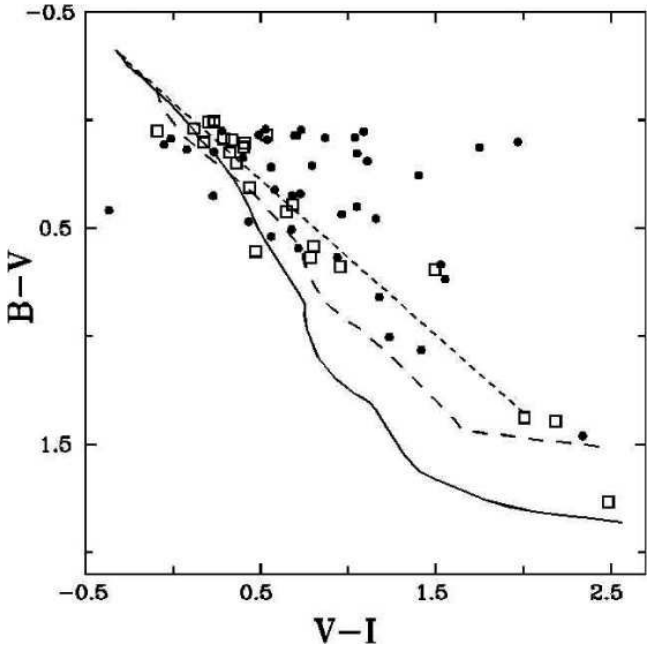

Fig. 2. The clouds of blended images (filled circles) and single blue objects (open squares) separated by a demarcation line (short-dashed) in colour-colour diagram. The zero-absorption lines for supergiants (solid) and Main-sequence stars (long-dashed) of Bessell (1990) are also drawn.

A measure for the contributions of fainter companions are the average differences Δ_V, Δ_I between the magnitudes of the brightest dominant component and those of the blended image. We found out that their typical values for the whole sample do not depend on the photometric passband and amount 0.5 both in V and I filters. However, if one composes two subsamples of blue and red 'stars' the determined average Δ_I would not be the same – respectively, 0.6 and 0.3 magnitudes. Let us note also that both Δ_V and Δ_I depend on magnitude – the brighter is the dominant star the smaller they are.

Due to decrease both of the extinction and of the flux contribution from fainter blue companions, the brightest RSGs ($I \sim 17^m$) are not strongly affected by blending – $\Delta_I \sim 0.15$ even in the crowded field of NGC 206.

These trends are evident from Table 1 and Table 2 where we compare the VI photometries of MLV, PM98 and HBOL for 12 red images (9 of them singular). Four of these objects should be Galactic dwarfs according to the photometric criterion for distinguishing RSGs used by PM98 (a demarcation curve in diagram $(B-V)$ vs. $(V-R)$). The Besancon model of the Milky Way predicts, however, only 0.25 foreground stars per arcmin^2 ($19. \leq V \leq 20.$, $2. \geq (V-I) \geq 1.8$ which gives one star in the area covered by WFPC2 of HST (≈ 4.3 arcmin^2). Passing to the neighboring bin ($2.2 \geq (V-I) \geq 2.$) the contamination drops almost three times. In order to clarify the issue we combined the VI magnitudes from HBOL with R magnitude from PM98 and plotted the suspected Galactic dwarfs with their colours in diagram $(V-R)$ vs. $(V-I)$. Only one of them lays over the zero-absorption line for Main-sequence stars (cf. Figure 6) and thus certainly belongs to the foreground while the other three seem to be RSGs. Thereby an incorrect discrimination between the RSG candidates in nearby galaxies and Milky Way dwarfs could be explained with the effect of blending.

Table 2. Blended red images from MLV and their indentification in PM98 and HBOL. The abbreviations are the same as in Table 1. The index 'tot, HST' denotes the integral magnitude of the components to which a 'star' from the MLV catalogue is resolved.

$\#_{\rm MLV}$	$\#_{\rm PM98}$	$\#_{\rm HBOL}$	I/C	R/F	$V_{\rm MLV}$	$V_{\rm PM98}$	$V_{\rm tot,\,HST}$	$I_{\rm MLV}$	$I_{\rm tot,\,HST}$
	97094		C		19.12		19.37	17.33	17.38
	781111	300026		fgd		19.50	19.75		17.45
		300123					21.03		21.18
		300566					22.70		22.44
		301995					23.80		22.44
		302603					24.01		22.72
		302958					24.12		22.69
103581			C		19.23		19.71	16.89	17.26
	78177	200032		fgd		20.38	19.87		17.32
		200735					22.86		22.73
		201535					23.50		21.87
		201951					23.69		23.35
		204291					24.34		23.01
		205765					24.81		21.40
104157			C		19.30		19.31	17.00	17.13
	781125	200033		fgd		19.82	19.88		17.24
		200090					20.79		20.82
		200637					22.70		22.68
		200654					22.74		22.42
		201259					23.34		21.14
		201839					23.66		22.14
		203313					24.11		22.38
		204458					24.38		22.79

2. Determination of the parameter R_V

A procedure of dereddening by means of the classical Q-method requires exact knowledge of the total-to-selective-extinction ratio $R_V = A(V)/E(B-V)$. Compiling data from various sources toward different lines of sight, CCM derived an uniform average extinction law $\langle A(\lambda)/A_V \rangle$ in the infrared, optical and ultraviolet spectral ranges as function of the wavelength and of R_V as a free parameter. The analytical formula is applicable for diverse conditions in the interstellar medium and could be used in absorption studies of diffuse as well of dense regions. It determines unambivalent relation between the reddening line slopes in colour-colour diagrams and R_V and thus allows observational estimate of this parameter. Below we expose two approaches for working out this task.

2.1. Test of the reddening line slope on different colour-colour diagrams

Let us denote the magnitudes measured in five different filters with m_1, m_2, m_3, m_4, m_5, and the colour excesses – with $E(m_1-m_2)$, $E(m_2-m_3)$, $E(m_3-m_4)$, $E(m_3-m_5)$. The extinction law derived by CCM gives the reddening line slopes $\kappa_{123} = E(m_1-m_2)/E(m_2-m_3)$, $\kappa_{234} = E(m_2-m_3)/E(m_3-m_4)$, $\kappa_{235} = E(m_2-m_3)/E(m_3-m_5)$ for every value of R_V and thus fixes the relations between these quantities. Naturally, two questions are rising: "Are these relations in accord with the empirical ones which may be obtained on base of the used stellar photometry? If yes, is this true for all possible values of R_V?" To find any answers we composed subsamples of blue stars from MLV which belong to two distinctive associations OB 48 and OB 78 and are identified with objects studied by Massey, Armandroff & Conti (1986). The identification provided independent UBV photometry making the obtained empirical relations $\kappa_{UBV} - \kappa_{BVR}$ and $\kappa_{UBV} - \kappa_{BVI}$ more reliable.

Our method consists of following steps.

1. Through the zero-absorption point of the earliest type stars (O5) in diagram $(U-B)$ vs. $(B-V)$ one draws a line with test value of the slope κ_{UBV} corresponding to particular value of R_V.
2. The identified stars within 1σ (the individual photometric error) from this line are selected.
3. The selected stars are plotted with their MLV photometry in diagrams $(B-V)$ vs. $(V-R)$ and $(B-V)$ vs. $(V-I)$ and one derives their less-squares fits through the zero-absorption points for O5-type stars.
4. The values of the fits' slopes are assigned respectively to κ_{BVR} and κ_{BVI}.

This procedure was repeated for different test slopes (different R_V's) and thus the desired empirical relations $\kappa_{UBV} - \kappa_{BVR}$ and $\kappa_{UBV} - \kappa_{BVI}$ were established. The results for OB 48 and OB 78 are plotted in Figure 3. One immediately sees that the obtained κ_{BVR} and κ_{BVR} do not vary substantially with the test slopes which perhaps reflects the lower precision of the MLV photometry. The value of κ_{UBV}, that corresponds to the intersection

point of the empirical curve and that derived by CCM, should be adopted as the most probable one. It is quite the same for both colour-colour diagrams and in both associations and gives on the average $R_V = 3.8 \pm 0.3$. The correctness of this estimate and its applicability for the entire galaxy were tested by use of another approach.

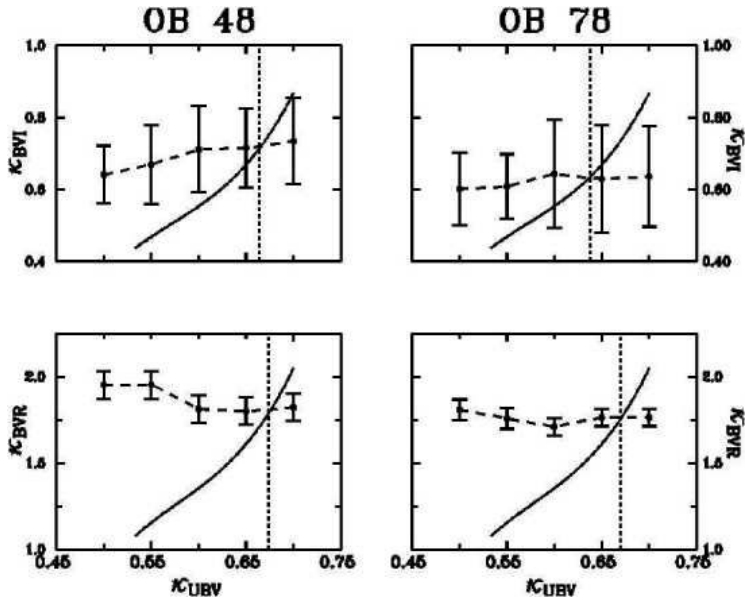

Fig. 3. The empirical relations $\kappa_{UBV} - \kappa_{BVR}$ (bottom panels) and $\kappa_{UBV} - \kappa_{BVI}$ (upper panels) for OB48 (left panels) and OB78 (right panels) obtained on the base of photometry of Massey, Armandroff & Conti (1986) and MLV. The results for different test slopes are marked with dots and connected with long-dashed line. The bars illustrate the errors of the less-square fits. The solid curve presents the calibrated relation of CCM while the short-dashed straight line shows the value of κ_{UBV} adopted by us.

2.2. A spectroscopy-based approach

Combining stellar photometry with knowledge of individual spectra, one is able to obtain estimates of the reddening slopes κ in colour-colour diagrams and hence – following CCM – of the individual R_V's. For this purpose we identified stars from the spectroscopic studies of Humphreys, Massey & Freedman (1990), MAP95 and PM98, with stars from our large sample with VI photometry. The procedure provided 18 objects of different spectral classes and 10 of them have a measured magnitude also in R filter. We derived their 'mixed' reddening slopes κ_{BVR} and κ_{BVI} using the more accurate BV photometry of Massey, Armandroff & Conti (1986) and PM98, and the RI magnitudes from MLV. Of course, the errors of photometry could yield significantly different individual slope values and therefore σ_κ

was calculated with varying the two colours within 1σ. The zero-absorption lines for supergiants were adopted from Bessell (1990) but their blue ends needed additional smoothing since the table points for early spectral types refer to different luminosity subclasses. Therefore we plotted several tracks of the Padova group (Fagotto et al. 1994) for Z=0.5 and for more massive stars ($> 15\ M_{\odot}$) which were transformed for colour-colour diagrams using the newest calibrations of Bessell, Castelli & Plez (1998). The blue post-Main-sequence parts of the tracks almost coincide which gives opportunity for correct fitting of the zero-absorption line. One should mention also their low metallicity dependence and thus the applicability of the derived fit to the conditions in M 31 (mean $Z \sim 0.04$).

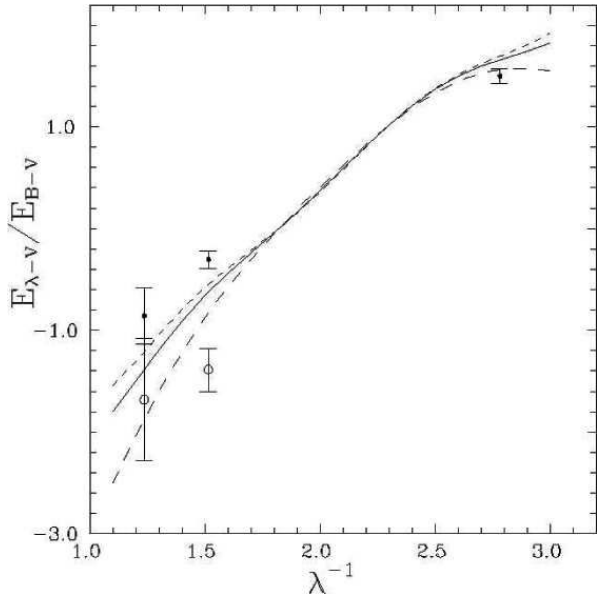

Fig. 4. Values of the median slopes in colour-colour diagrams for early-type (filled circles) and red stars (open circles) with spectroscopy of Humphreys, Massey & Freedman (1990), MAP95 and PM98. Three curves calculated by use of the CCM formula are plotted for comparison – for $R_V = 3.0$ (short-dashed line),for $R_V = 6.0$ (long-dashed line) and for $R_V = 3.8$ (solid line).

We have divided the identified objects in two subsamples: early-type (A-F) and red (K-M) stars. For particular wavelength λ^{-1} were retained only those stars which give a plausible (positive) slope with not a large error. Due to the small number of objects remaining it is appropriate to adopt the median value $\kappa_{\rm med}$ as the average one for the corresponding group whereas the average value of κ_{UBV} is taken directly from MAP95. In Figure 4 the results are compared with the curves derived by CCM for fixed values of R_V. The picture illustrates the range of possible total-to-selective-extinction

ratios which obviously embraces the estimate from the previous subsection (solid line). In order to derive R_V more accurately, we varied this parameter with step 0.1 and performed χ^2 minimization of the individual slopes' deviations from the extinction law of CCM. As seen from Figure 5, this method gives exactly and unambiguously $R_V = 3.8$ which is also confirmed by minimization of the deviations of $\kappa_{\rm med}$ for both subsamples and filter wavelengths. One gets some idea about the uncertainties of this approach by applying the procedure to the deviations of the *arithmetic averaged* values $\kappa_{\rm aa}$. Finding the corresponding $R_V = 3.4$, we will adopt $R_V = 3.8 \pm 0.4$ as fixed total-to-selective-extinction ratio in all regions of M 31.

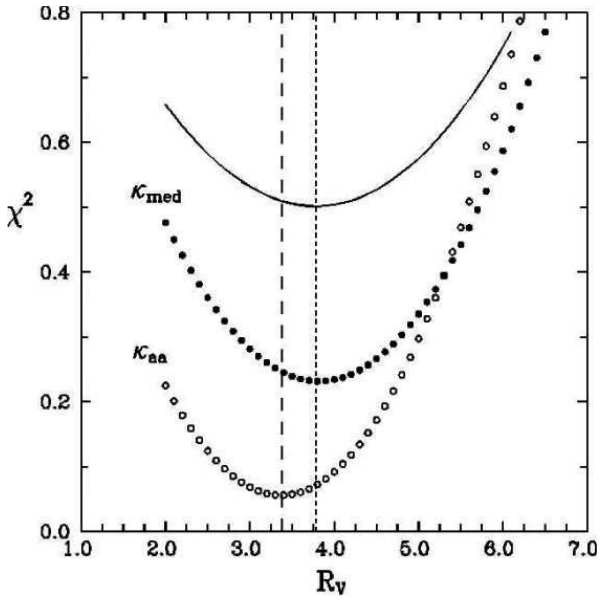

Fig. 5. Toward determination of R_V using χ^2 minimization. The solid curve represents the χ^2 sum of the individual slopes' deviations from the CCM law as function of R_V (normalized arbitrarily for demonstrativeness) whereas the behaviour of this quantity for the deviations of $\kappa_{\rm med}$ and $\kappa_{\rm aa}$ is illustrated respectively with filled and with open circles. See text.

3. Dereddening of blue stars and RSG candidates

The typical completeness limit $V_{\rm lim} = 20.7$ of the blue stars' sample was obtained comparing the apparent luminosity function with that of the identified stars from Massey, Armandroff & Conti (1986). An analogical approach with reference to objects from PM98 leads to $V_{\rm lim} = 19.5$ for our sample of red stars. Therefore only stars with $V \leq 20.0$ were selected for dereddening – the more so as the list of fainter blue and red objects suffers

both from blending and from significant foreground contamination. This selection restricts our absorption study to the younger massive population of M 31 (top-of-the-Main-sequence stars and supergiants) which may have some intrinsic extinction due to existing envelopes. Preliminary differential dereddening for the Milky Way was performed for each star of the samples with the 'standard' value of $R_V = 3.1$. In this procedure the excess $E(B-V)$ was determined as function of the position in field of M 31 using the average Galactic reddening estimates of Burstein & Heiles (1984) for nearby areas on the sky. Its value varies from 0.06 at the southern edge and 0.10 at the northern edge of the galaxy.

3.1. The standard Q-method

Magnier et al. (1997) show that the adoption of single constant extinction value is a too rough approximation even within M 31 OB associations where A_V varies in large ranges. Nevertheless, Haiman et al. (1994b) do not perform differential dereddening with the MLV data overestimating, in our view, the significance of the photometric errors. As we have demonstrated in previous section, the proper treatment of the blending effect still enables the classical approach of differential extinction derivation.

By means of the Q-method 1231 blue stars plotted on diagram $(B-V)$ vs. $(V-I)$ were dereddened individually to the zero-absorption lines for supergiants and dwarfs of Bessell (1990). Then, comparing the assumed positions of each star in colour-luminosity diagram in both cases, we elaborated a simple procedure for distinguishing the Main-sequence members and for adopting of appropriate extinction values. Stars under the reddening line for spectral type A5 (with slope corresponding to the adopted value of $R_V = 3.8$) and over the demarcation line between the clouds of singular and blended images (see Figure 2) were preliminarily excluded from the sample. Juxtaposing the stellar counts in diagram $(B-V)$ vs. $(V-I)$ with predictions of the Besancon model of the Galaxy, one finds possible foreground contamination in several bins which amounts $\sim 5\%$ of the whole sample. We did not take into consideration objects with position under the 'red tail' of the zero-absorption line in order to avoid ambiguity in some dereddening estimates. Thereby an upper limit for the calculated extinctions was set. To diminish the number of fake blue stars, we excluded also dereddened objects with positions in diagram M_V vs. $(V-I)_0$ more than 1σ over the track for 40 $M_\odot$. Stars with 'negative excesses' were retained in the sample except those with unplausibly blue colours (e.g. $(B-V) < -0.5$).

We obtained also the extinction for 113 red stars applying the Q-method in diagram $(V-R)$ vs. $(V-I)$. The initial sample was composed by selection of red objects with V > 17. which lay under and in 1σ around the zero-absorption line for supergiants. Their number was restricted further by the leftmost possible reddening line (see Figure 6) which determines the spectral types to be no earlier than K6. The true colours of K6 were assigned also to objects which lay within 1σ to the left of that line. After applying the Besancon model to diagram $(V-R)$ vs. $(V-I)$, it turned out that our sample could be considered free from foreground contamination. The positioning of identified stars from PM98 in this diagram (Figure 6) provides another check of the latter suggestion. The magnitudes in V and R filters of PM98 were

supplemented with the magnitude in I band from MLV. Although in the area of earlier spectral classes the Galactic dwarfs and RSGs of M 31 (as classified by Massey) are well mixed, one may see that is not the case with our sample. Several foreground stars lay close and below the zero-absorption line for supergiants but within the range of photometric errors.

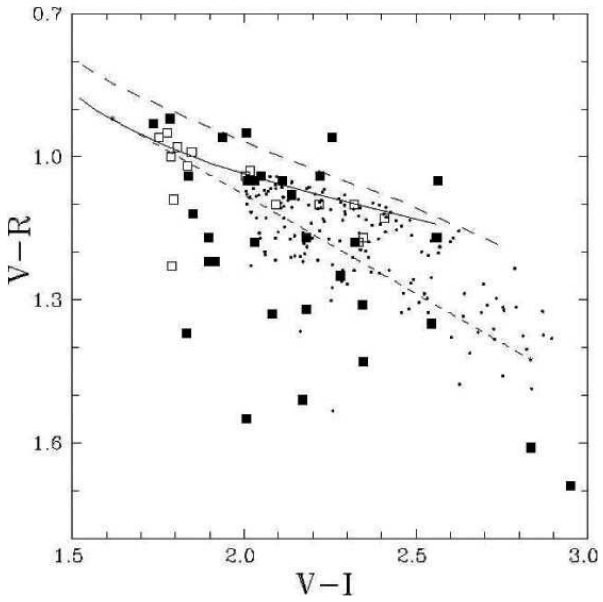

Fig. 6. Colour-colour diagram with the positions of 113 RSG candidates (dots) which were to be dereddened by means of the Q-method. The zero-absorption lines for supergiants (solid) and dwarfs (long-dashed) are drawn together with the leftmost possible reddening line (short-dashed) which corresponds to spectral class K6. The position of identified foreground stars (open squares) and supergiants of M 31 (filled squares) from PM98 are plotted using I-band magnitudes from MLV.

The absolute magnitude M_V of all dereddened stars was calculated with distance modulus 24.47 (Stanek & Garnavich 1998). The correlation between M_V and the derived total extinction A_V is shown in Figure 7. The well pronounced upper boundary corresponds to the limits of photometry. The distributions for both blue and red samples are practically the same but the former one exhibits much larger dispersion toward its more luminous tail. That points probably to the variety of ages and respectively to different conditions in the circumstellar environment of the massive blue stars.

3.2. The 'closest-neighbors approach'

In view of our goal to select more RSG candidates in M 31 with known luminosity we composed for dereddening a larger sample of 839 stars with VI

photometry only. Their magnitudes and colours were in range $17. \leq V \leq 20.$, $2. \leq (V-I) \leq 3.$ which ensures a vanishing percentage of Galactic dwarfs (with the only exception in the bin $V > 18.$, $(V-I) < 2.2$, where it reaches 25%). We looked up to find close neighbors among the dereddened blue stars for each object of this sample. Obtaining lists of 98 stars with neighbor(s) within radius of 5 arcsec and 192 stars with neighbor(s) within radius of 10 arcsec, we assigned to them the median extinction value of their neighbors. This estimate makes sense since such angular distances correspond to sizes twice less than the mean size of Andromeda's OB associations (Ivanov 1996) to which most of our blue stars belong.

4. Selection of RSG candidates in M 31

4.1. Previous photometric and spectroscopic Studies

The most eminent results in search for RSGs in Andromeda galaxy were achieved in the last decade by Humphreys et al. (1988) and PM98. The former work is based mainly on photographic photometry of Berkhuijsen et al. (1988) and contains lists of 42 Galactic dwarfs and 23 late-type supergiants selected through spectroscopic criteria and an analysis of diagram $(J-H)$ vs. $(H-K)$. Since the completeness limits are as high as $V \approx 18.8$, $R \approx 17.8$, that study concerns only the brighter RSG candidates. A deeper survey of red stars in M 31 presented Nedialkov, Kourtev & Ivanov (1989) who used B and V plates obtained with an 2 m RCC telescope and composed their sample (46 stars) by blinking and selecting of objects with $(B-V) > 1.8$. Their results support the claim about lack of bright RSGs in this galaxy and especially in its southwestern part. This statement was repeated again by PM98. Using BVR CCD photometry on a 2.1 m telescope and plotting the objects in the colour-colour diagram, he distinguished successfully 102 RSG candidates from 99 foreground stars. Ten RSGs are confirmed also spectroscopically and exhibit spectral classes from K5 to M2.5. The completeness limit of $V = 20.5$ enables the visibility of M supergiants with absolute magnitudes $M_V \approx -4.5$ and thus makes the catalogue of PM98 an appropriate reference frame for our selection.

4.2. Our lists of RSG candidates

In Table 3 we have put all dereddened by means of the Q-method RSG candidates with their absolute magnitudes, true colours, extinctions and identifications, in comparison with the works already cited. The first overview shows that we propose 60 new candidates for RSGs which could not be found in the previously refered works. Among the identified ones it is worth to note R-23, R-53 and R-95 from the catalogue of Humphreys et al. (1988) whose luminosity class is confirmed spectroscopically. The cross-identification with objects from PM98 is very poor (only 2 RSGs) but that may well be explained with the small total area of the fields observed by Massey: 2.3% of the region covered by the VRI photometry of MLV. The most massive RSG candidates and their relative number deserve special attention in view of the claim in PM98 that the most luminous of them originate as stars of

$\sim$ 13-15 $M_\odot$. We composed diagram M_V vs. $(V-I)_0$ with tracks of the Padova group (Fagotto et al. 1994) (transformed to colours, as already mentioned, with the calibrations of Bessell, Castelli & Plez (1998)) and selected all dereddened stars over the track with initial mass 20 $M_\odot$ as illustrated in Figure 8. Since the extinction of some of them is derived by means of the 'closest neighbors-approach' its value – and hence the derived mass range and luminosity – could be incorrect. Therefore we included in this list only evolved objects with spectral class M ($(V-I)_0 > 1.8$). The selected 68 RSG candidates are listed in Table 4. Because of their positions in diagram V vs. $(V-I)$ ($(V-I) > 2.2$; see Section 2.2) one can be sure none of them is a foreground dwarf.

5. Discussion

The full list of selected RSG candidates with derived A_V suffers from significant incompleteness even in the range of largest luminosities. The reason lies in the problems MLV obviously had had with the photometry in R filter. A half of the red stars identified with RSGs from PM98 and with typical values of $(V-I)$ have a measured magnitude in R which corresponds to negative $(V-R)$ colours. That restricted, of course, the number of RSG candidates to be dereddened by means of the Q-method and diminished indirectly the effectiveness of the 'closest-neighbors approach'. A convincing illustration of this fact provides Figure 9 where we juxtapose the luminosity function

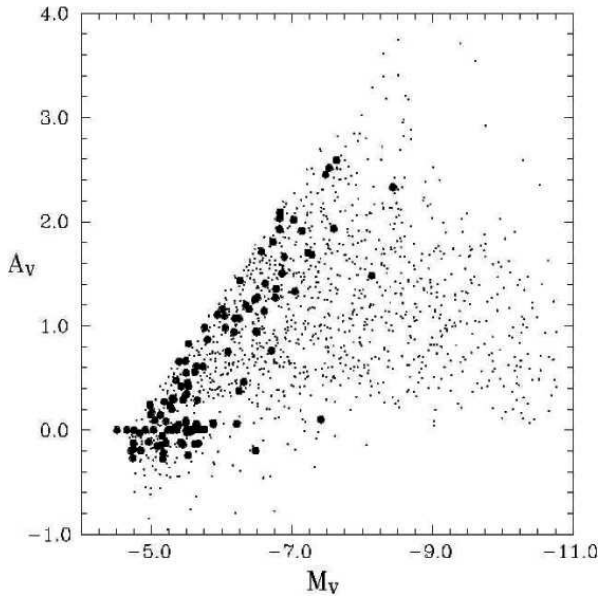

Fig. 7. The correlation 'absolute magnitude - total extinction' for red (filled circles) and blue stars (dots) dereddened by means of the Q-method.

of all dereddened red stars (solid line) with that of the 839 RSG candidates with VI photometry (dashed line). We ascribed an average value $A_V = 1.0$ to objects whose extinction we were not not able to derive individually – an estimate, which is close to the median values for several OB associations studied by Magnier et al. (1997). A single look at Figure 9 reveals that in most of the bins we have 'lost' about 50% of the RSG candidates because of lack of a close neighbor. Comparing the luminosity function of all potential RSG candidates (839 objects) with Figure 15 in PM98 and normalizing the numbers in each bin to the area of his fields, we come to the conclusion that the completeness in our work is similar and even better in range $M_V = -7.5$ to -5.0.

It is worth to look intently at the shape of the obtained apparent luminosity function of the RSGs. It differs from Massey's result for Andromeda galaxy and resembles much more the cases in other Local Group galaxies (see Figure 15 in PM98). The presented in PM98 distributions for M 31, M 33 and NGC 6822 were interpreted there in terms of the "Conti scenario" (Conti 1976) for formation of Wolf-Rayet stars through stellar wind – the higher is the metallicity Z the higher should be the mass-loss rate and the shorter time the star would spent in the RSG stage. Hence, in galaxies with

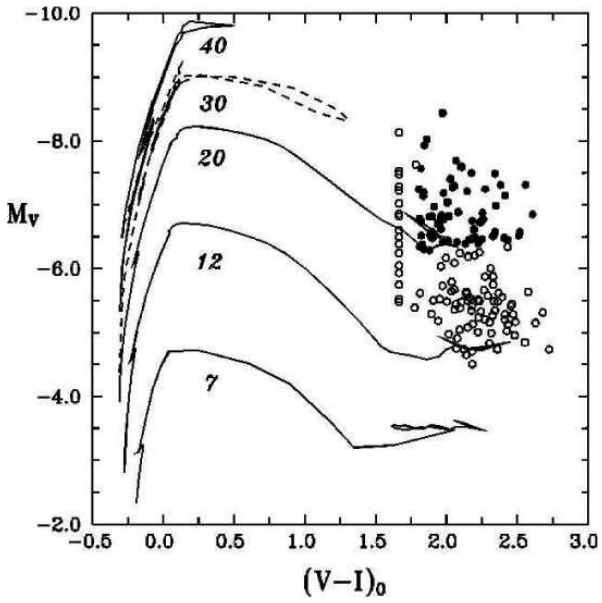

Fig. 8. The RSG candidates from our selections in diagram M_V vs. $(V-I)_0$. The stellar masses in units $[M_\odot]$ are indicated below the corresponding track. The RSG candidates from Table 3 are marked with open circles and all dereddened stars over 20 $M_\odot$ (Table 4) – with filled circles. The group of points with one and the same $(V-I)_0 = 1.664$ consists of stars to which all the true colour of spectral type K6 was ascribed (see Section 4.1). The track of a 30 $M_\odot$ star (dashed line) is calculated for lower metallicity $Z = 0.02$ (than the typical one for M 31) and is plotted for comparison only.

high metal abundance, one has to expect rather sharp decrease of RSGs' number with increasing luminosity than extended tails of the distribution. Our result for M 31 casts doubt on that assumption. We suppose that the steep luminosity function of RSGs derived by PM98 is conditioned by applying small fixed values of colour excess $E(B-V)$ for each field (in the range between 0.08 and 0.25). Taking also into account the adopted in that work lower value of $R_V = 3.2$, it is easy to explain the claimed paucity of RSGs over $M_V = -6.0$ and their 'concentration' in three bins down to $M_V = -4.0$. We believe that the differential dereddening we performed – although of a limited sample – leads to more accurate determination of the RSGs' absolute magnitudes and reproduces more correctly their luminosity function.

Looking back at Figure 8 and Table 4, we can state with certainty that in M 31 exists a significant number of RSGs whose progenitors should have masses over 20 $M_\odot$. This result is in accord with the latest investigations of Massey & Johnson (1998) who found distinctive spatial correlation between the luminous RSGs and Wolf-Rayet stars in this galaxy – a fact which testifies that stars with initial masses over 15 $M_\odot$ still undergo the phase of RSG in their evolution. The completeness limit of our sample (cf. Figure 9), however, hinders us to estimate the relative duration of this phase in comparison with the lifetime of RSGs of lower mass.

Conclusions

Our main result in the recent work is the derivation of a new value of the total-to-selective-extinction ratio in M 31 $R_V = 3.8 \pm 0.4$ obtained by

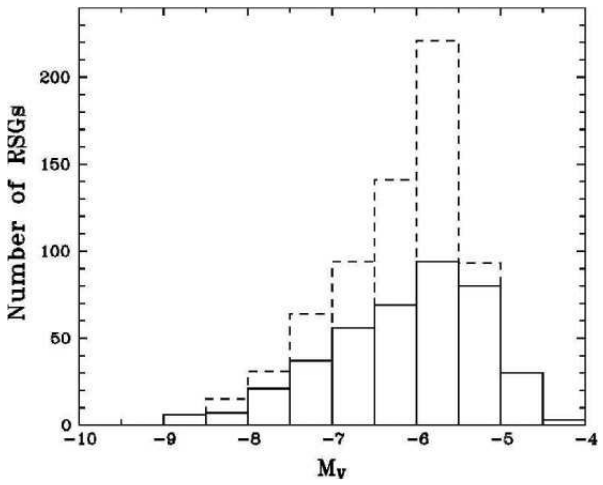

Fig. 9. The luminosity function of all dereddened RSG candidates (solid line) and that of the full list of 839 stars with $17. \leq V \leq 20.$, $2. \leq (V-I) \leq 3.$ (dashed line). An average value $A_V = 1.0$ was ascribed to objects whose extinction we were not able to derive individually.

means of two different methods. This estimate is considerably higher than the previous results of Kron & Mayall (1960) and Martin & Shawl (1978) but still it is within 2σ from the 'standard' value $R_V = 3.2$ adopted in PM98. Nevertheless, we have reasons to infer that the extinction law in Andromeda galaxy differs from that in the Milky Way. Additional hints in this direction gives the work of MAP95 albeit their calculations of the average reddening line slope lead – applying the formula of CCM – to a very large and thus questionable value of R_V ($\sim 10.$). Larger values of R_V may indicate leftover remnants of molecular clouds which surround the young stars.

The obtained averaged colour excesses and total extinctions for blue and red luminous stars in M 31 are in good agreement with the newest results for several OB associations (Magnier et al. 1997). We should point out that most of the selected young objects belong to the spiral arms where much dust is concentrated whereas it is hard to distinguish possible interarm stars because of the highly inclined galactic plane. If the calculated extinctions are corrected for the line of sight, they lead to significantly lower optical depths than the estimates of Nedialkov (1998) for the spiral arms ($\tau_B \sim 4.$). Therefore one is not allowed – without certain assumptions about the gas-to-star geometry – to interpret our results as a subsequent objection (see e.g. Disney et al. 1989, Valentijn 1990) against the claimed optical transparency of the spirals.

The selected 113 RSG candidates with accurately derived extinction and luminosity build up the largest up-to-date list of such objects in M 31. Sixty of them are not identified in the works refered here and offer interesting possibilities for further spectroscopic studies. We composed also two lists of other RSG candidates with extinction calculated using the results for their closest neighbors (within 5 and 10 arcsec). These lists contain correspondingly 98 and 192 objects and are available in electronic form upon request. From the three mentioned lists were extracted 68 stars with masses presumably over 20 $M_\odot$. Their relative number and the shape of their luminosity function suggest that the massive stars' evolution in M 31 follows the same pattern as in the other Local Group galaxies without any distinctive influence of the metallicity.

This research has made use of SIMBAD database operated at CDS, Strasbourg, France. We are grateful to Dr. Valentin Ivanov for the helpful notes which improved this paper. Our work is part of the project AZ. 940.4-326 of the Union der Deutschen Akademien der Wissenschaften and it was supported by a grant of the Bulgarian Science Foundation.

References

Berkhuijsen, E., Humphreys, R., Ghigo, F., & Zumach, W., 1988, *A&AS*, 76, 65
Bessell, M., 1990, *PASP*, 102, 1181
Bessell, M., Castelli, F., & Plez, B., 1998, *A&A*, 333, 231
Bianchi, L., Clayton, G., Bohlin, R., Hutchings, J., & Massey, P., 1996, *ApJ*, 471, 203
Burstein, D., & Heiles, C., 1984, *ApJS*, 54, 33
Cardelli, J., Clayton, G., & Mathis, J., 1989, *ApJ*, 345, 245 (CCM)
Chiosi, C., & Maeder, A., 1986, *ARA&A*, 24, 329
Conti, P., 1976, *Mem. Soc. Roy. Sci. Liege*, 6^e, Ser. 9, 193
Disney, M., Davies, J., & Phillipps, S., 1989, *MNRAS*, 239, 939
Efremov, Yu., Ivanov, G., & Nikolov, N., 1987, *Ap&SS*, 135, 119
Fagotto, F., Bressan, A., Bertelli, G., & Chiosi, C., 1994, *A&AS*, 104, 365

Haiman, Z., Magnier, E., Lewin, W., Lester, R., van Paradijs, J., Hasinger, G., Pietsch, W., Supper, R., & Truemper, J., 1994a, *A&A*, 286, 725
Haiman, Z., Magnier, E., Battinelli, P., Lewin, W., van Paradijs, J., Hasinger, G., Pietsch, W., Supper, R., & Truemper, J., 1994b, *A&A*, 290, 371
Humphreys, R., Massey, P., & Freedman, W., 1990, *AJ*, 99, 84
Humphreys, R., Pennington, R., Jones, T., & Ghigo, F., 1988, *AJ*, 96, 1884
Hunter, D., Baum, W., O'Neil Jr., E., & Lynds, R., 1996, *ApJ*, 468, 633 (HBOL)
Ivanov, G., 1996, *A&A*, 305, 708
Kron, G., & Mayall, N., 1960, *AJ*, 65, 581
Kudritzki, R., Pauldrach, A., Puls, J., & Abbot, D., 1989, *A&A*, 219, 205
Magnier, E., Lewin, W., van Paradijs, J., Hasinger, G., Jain, A., Pietsch, W., & Truemper, J., 1992, *A&AS*, 96, 379 (MLV)
Magnier, E., Hodge, P., Battinelli, P., Lewin, W., & van Paradijs, J., 1997, *MNRAS*, 292, 490
Martin, P., & Shawl, S., 1978, *ApJ*, 253, 86
Massey, P., 1998, *ApJ*, 501, 153 (PM98)
Massey, P., Armandroff, T., & Conti, P., 1986, *AJ*, 92, 1303
Massey, P., Armandroff, T., Pyke, R., Patel, K., & Wilson, C., 1995, *AJ*, 110, 2715 (MAP95)
Massey, P., & Johnson, O., 1998, *ApJ*, 505, 793
Mochejska, B., Macri, L., Sasselov, D., Stanek, K., 2000, *AJ*, 120, 810
Nedialkov, P., 1998, *Ph.D. thesis*, University of Sofia, Bulgaria
Nedialkov, P., Kourtev, R., & Ivanov, G., 1989, *Ap&SS*, 162, 1
Ratnatunga, K., & Bahcall, J., 1985, *ApJS*, 59, 63
Robin, A., 1994, *Ap&SS*, 217, 163
Schechter, P., Mateo, M., & Saha, A., 1993, *PASP*, 105, 1342
Stanek, K., & Garnavich, P., 1998, *ApJ*, 503, 131
Valentijn, E., 1990, *Nature*, 346, 153
Valentijn, E., 1994, *MNRAS*, 266, 614
van den Bergh, S., 1968, *Observatory*, 88, 168
Veltchev, T., Nedialkov, P., & Ivanov, G., 1999, *RevMexAA*, 35, 13
Zaritsky, D., Kennicutt, R., Jr., & Huchra, J., 1994, *ApJ*, 420, 87

Appendix A: RSG candidates in M 31

Table 3: Full list of 113 RSG candidates in M31 with extinction derived by means of the Q-method. In the last four columns are given the identifications with other works as follows: B88 – Berkhuijsen et al. (1988), H88 – Humphreys et al. (1988), Sp – spectral classification according to H88 (if an asterisk follows – according to PM98), N89 – Nedialkov, Kourtev & Ivanov (1989).

Nr. in MLV	Coordinates 2000.0		M_V	V	$(V-I)_0$	A_V	B88	H88	Sp	N89
417577	11.118438	41.858448	-8.437	18.607	1.972	2.329	—	—	—	R22
437031	11.638994	41.997456	-8.134	18.068	1.664	1.482	41-4953	R-23	M0	R39
327891	11.241807	41.514965	-7.631	19.662	1.784	2.591	—	—	—	—
436447	11.634009	41.993141	-7.591	19.063	2.106	1.934	41-4926	—	—	—
267939	11.132378	41.318951	-7.528	19.682	1.664	2.515	—	—	—	—
242943	10.927945	41.245186	-7.476	19.669	1.664	2.452	—	—	—	—
320145	11.160924	41.492786	-7.407	17.396	2.027	0.102	41-2911	R-95	M1/M2	R20
114840	10.644233	40.807350	-7.281	19.080	1.664	1.682	40-4173	—	—	—
417341	11.512323	41.857262	-7.226	19.191	1.664	1.702	41-4584	R-53	K5-M0	R35
136803	10.543445	40.924122	-7.141	19.452	1.836	1.910	40-3947	—	—	—
102137	10.196411	40.745743	-7.039	18.970	2.006	1.331	40-2401	R-30	—	—
424878	11.241183	41.901272	-7.023	19.712	1.664	2.018	—	—	—	—
229986	10.941835	41.194000	-6.888	19.466	2.083	1.662	40-4653	—	—	—
417824	11.517426	41.859756	-6.855	19.362	1.664	1.502	41-4606	—	—	—
82288	9.975927	40.667858	-6.826	19.938	1.965	2.089	—	—	—	—
226779	10.472175	41.178951	-6.821	19.796	1.664	1.926	—	—	—	—
139447	10.626180	40.940041	-6.817	19.897	1.897	2.030	—	—	—	—
285099	11.122199	41.385464	-6.774	19.281	2.259	1.357	41-2658	R-110	—	—
380803	11.321597	41.663338	-6.763	19.215	1.959	1.270	41-3867	—	M2.5*	—
249017	10.446620	41.260513	-6.728	19.772	2.237	1.807	—	—	—	—
223296	10.506104	41.171646	-6.706	18.747	1.941	0.762	—	—	—	—
211171	10.330422	41.143433	-6.615	19.479	2.194	1.405	—	—	—	—
179741	10.185312	41.064186	-6.601	19.227	1.664	1.141	40-2353	—	—	—
206402	10.264723	41.130531	-6.564	19.836	1.900	1.711	—	—	—	—
263242	11.065625	41.297363	-6.506	19.458	2.329	1.270	—	—	—	—
132491	10.204449	40.902920	-6.498	19.120	1.664	0.936	—	—	—	—
228566	10.824341	41.187141	-6.485	19.153	1.900	0.947	—	—	—	—
232974	10.409659	41.208912	-6.480	18.016	2.409	0.000	—	—	—	—
293476	11.126873	41.409916	-6.471	19.482	2.183	1.255	—	R-105	—	—
432205	11.571004	41.955662	-6.386	19.496	1.664	1.163	41-4772	—	—	—
286600	11.103818	41.389507	-6.341	19.556	2.432	1.199	—	—	—	—
232548	10.820907	41.206753	-6.309	18.841	1.840	0.458	—	—	—	—
158388	10.778870	41.010559	-6.256	19.865	2.233	1.435	—	—	—	—
237038	10.392576	41.226608	-6.245	18.826	2.094	0.378	40-3411	—	—	—
112308	10.588814	40.792923	-6.244	19.504	1.664	1.069	40-4062	—	—	—
128032	10.563226	40.876427	-6.208	18.534	2.201	0.061	40-4007	—	—	—
395378	11.343620	41.753620	-6.188	19.597	2.153	1.074	—	—	—	—
103581	10.127163	40.750854	-6.169	19.448	1.996	0.939	—	—	—	—
87586	9.998288	40.687634	-6.088	19.341	2.056	0.753	40-1221	—	—	—
140965	10.386338	40.949303	-6.048	19.617	1.664	0.981	40-3380	—	—	—
222028	10.299899	41.169147	-6.037	19.749	1.961	1.096	40-2958	—	—	—
325905	11.232757	41.509697	-6.005	19.857	2.312	1.160	—	—	—	—
361623	11.197263	41.607555	-5.933	19.878	1.664	1.105	—	—	—	—
79609	9.957870	40.653870	-5.879	18.864	2.330	0.068	40-1036	—	—	—
168036	10.260784	41.035225	-5.877	18.867	2.274	0.057	40-2744	—	—	—
311354	10.867110	41.469021	-5.793	19.774	2.037	0.867	—	—	—	—
289265	10.709546	41.397305	-5.753	18.953	2.330	0.008	—	—	—	—
139352	10.426512	40.939457	-5.750	19.917	1.664	0.984	—	—	—	—
42157	10.158985	40.467342	-5.729	19.551	1.972	0.610	—	—	—	—
83997	10.192136	40.674118	-5.674	19.010	2.056	0.008	40-2381	—	—	—
407528	11.580252	41.809811	-5.665	18.921	2.266	0.000	41-4793	—	—	—
73184	10.237486	40.622486	-5.648	19.313	2.035	0.287	40-2610	—	—	—
116736	10.082007	40.819996	-5.639	19.654	2.139	0.613	40-1627	—	—	—
393691	10.935226	41.744274	-5.637	19.133	2.579	0.059	—	—	—	—
105384	10.137760	40.757343	-5.617	19.619	1.813	0.558	—	—	—	—
228468	10.940392	41.186668	-5.616	18.942	2.368	0.000	40-4651	—	—	—
297393	10.881673	41.422993	-5.608	18.862	2.138	0.000	—	—	—	—
66706	9.936619	40.595116	-5.578	18.892	2.293	0.000	40-0926	—	—	—
262935	10.561402	41.296246	-5.557	18.913	2.393	0.000	—	—	—	—

Continued on next page

Table 3 – *Continued from previous page*

Nr. in MLV	Coordinates 2000.0		M_V	V	$(V-I)_0$	A_V	B88	H88	Sp	N89
197557	10.211429	41.103188	-5.548	19.123	2.163	0.000	—	—	—	—
422806	11.153700	41.888088	-5.524	19.614	1.952	0.422	—	—	—	—
209021	10.869518	41.137890	-5.522	19.996	1.664	0.828	—	—	—	—
195456	10.403613	41.097816	-5.517	18.932	2.178	0.240	—	—	—	—
199087	10.375803	41.107571	-5.511	19.632	2.224	0.454	—	—	—	—
367762	11.166618	41.623421	-5.501	19.556	1.907	0.350	41-2941	—	—	—
353326	11.382848	41.586491	-5.498	19.184	2.150	0.000	41-4132	—	—	—
185612	10.709586	41.077473	-5.494	18.976	2.233	0.000	40-4282	—	—	—
190260	10.606122	41.085457	-5.491	19.746	2.336	0.549	—	—	—	—
117794	10.085511	40.826340	-5.488	19.283	2.363	0.091	—	—	—	—
232722	10.406325	41.207687	-5.484	19.276	2.002	0.068	—	—	—	—
278708	11.129682	41.371151	-5.481	19.553	2.106	0.336	—	—	—	—
323709	10.772453	41.502758	-5.480	19.885	1.664	0.663	—	—	—	—
97783	10.111373	40.729416	-5.447	19.521	2.463	0.290	—	—	M2.5*	—
85372	10.249909	40.678814	-5.443	19.095	2.066	0.000	—	—	—	—
367024	10.983985	41.621540	-5.420	19.705	2.181	0.418	41-1966	—	—	—
138565	10.652536	40.934727	-5.412	19.157	2.456	0.000	40-4189	—	—	—
138664	10.549353	40.935265	-5.390	19.953	1.775	0.660	—	—	—	—
55552	10.285732	40.548210	-5.382	19.342	2.095	0.051	40-2877	—	—	—
455055	11.441019	42.170864	-5.361	19.109	2.058	0.000	41-4365	—	—	—
329364	11.282765	41.519047	-5.346	19.833	2.342	0.476	—	—	—	—
354873	11.363120	41.590343	-5.342	19.394	2.176	0.031	41-4061	—	—	—
155336	10.287796	41.002903	-5.331	19.376	2.243	0.021	40-2892	—	—	—
369008	11.265914	41.626938	-5.315	19.687	2.679	0.296	41-3567	—	—	—
99714	10.143638	40.736904	-5.293	19.687	1.894	0.303	—	—	—	—
39305	10.097602	40.448238	-5.287	19.583	2.470	0.200	40-1734	—	—	—
90048	10.176888	40.697567	-5.282	19.188	2.413	0.000	40-2307	—	—	—
207758	10.202614	41.134407	-5.265	19.657	2.326	0.232	40-2439	—	—	—
375993	10.910624	41.647476	-5.233	19.237	2.227	0.000	41-1660	—	—	—
41254	10.032395	40.461670	-5.204	19.340	2.272	0.000	40-1384	—	—	R14
393714	11.218287	41.744453	-5.203	19.593	2.412	0.085	41-3287	—	—	—
255049	11.021120	41.272854	-5.181	19.786	1.942	0.273	—	—	—	—
374507	11.112427	41.642986	-5.165	19.322	2.486	0.000	41-2584	—	—	—
324841	11.023012	41.506336	-5.160	19.267	2.306	0.000	—	—	—	—
386660	11.047344	41.699619	-5.149	19.504	2.629	0.000	41-2273	—	—	—
83954	10.447381	40.673985	-5.134	19.396	2.188	0.000	40-3643	—	—	—
341285	10.808848	41.553654	-5.123	19.726	2.434	0.145	—	—	—	—
315505	10.572876	41.480328	-5.079	19.467	2.149	0.000	41-0654	—	—	—
185034	10.516809	41.076214	-5.044	19.740	2.092	0.096	—	—	—	—
319142	11.243835	41.490154	-5.026	19.444	2.426	0.000	41-3440	—	—	—
367602	11.292324	41.622997	-5.004	19.881	2.222	0.178	—	—	—	—
131833	10.738815	40.899723	-4.989	19.841	2.318	0.148	—	—	—	—
309865	10.862050	41.465076	-4.976	19.970	2.016	0.246	—	—	—	—
282770	11.096257	41.379726	-4.959	19.626	2.482	0.000	—	—	—	—
364310	10.908365	41.614582	-4.910	19.560	2.076	0.000	41-1646	—	—	—
170917	10.766940	41.043056	-4.842	19.649	2.554	0.000	—	—	—	—
268712	10.472554	41.323277	-4.828	19.839	2.304	0.000	—	—	—	—
363136	11.262823	41.611610	-4.748	19.957	2.069	0.000	—	—	—	—
402905	11.181502	41.788925	-4.740	19.846	2.123	0.000	—	—	—	—
266681	11.039278	41.311646	-4.740	19.771	2.359	0.000	—	—	—	—
234160	10.834925	41.214603	-4.734	19.688	2.724	0.000	—	—	—	—
139081	10.359098	40.937881	-4.706	19.779	2.181	0.000	40-3255	—	—	—
196944	10.448886	41.101601	-4.649	19.821	2.140	0.000	—	—	—	—
102808	10.292471	40.748173	-4.506	19.964	2.182	0.000	—	—	—	—

Table 4: RSG candidates in M31 whose progenitors should have masses over $20M_{\odot}$). The abbreviations are the same as in Table 3. The 8th column with designation 'E' denotes the method of extinction derivation as follows: Q– Q-method, A – 'closest-neighbors-approach' within 5 arcsec, B – 'closest-neighbors-approach' within 10 arcsec.

Nr. in MLV	Coordinates 2000.0		M_V	V	$(V-I)_0$	A_V	E	B88	H88	Sp	N89
417577	11.118438	41.858448	-8.437	18.607	1.972	2.329	Q	—	—	—	R22
5370	9.887635	40.151890	-8.024	18.093	1.860	1.647	B	39-0998	—	—	—
30186	9.965296	40.380390	-7.932	18.962	1.844	2.424	A	—	—	—	—
130350	10.390935	40.892464	-7.690	18.130	2.067	1.350	B	40-3404	—	—	—
436447	11.634009	41.993141	-7.591	19.063	2.106	1.934	Q	41-4926	—	—	—
351497	11.399905	41.581776	-7.567	17.464	1.820	0.561	B	41-4215	R-88	—	—
256709	10.394132	41.277287	-7.497	17.682	2.175	0.709	B	41-0214	R-175	M3	—
129360	9.963593	40.884216	-7.486	18.407	2.343	1.423	B	40-1063	IIIR-2	—	R11
320145	11.160924	41.492786	-7.407	17.396	2.027	0.102	Q	41-2911	R-95	M1/M2	R20
304588	11.113409	41.448463	-7.312	18.241	2.558	1.082	B	—	—	—	—
11684	9.857494	40.236900	-7.308	18.833	2.383	1.671	B	—	—	—	—
106445	10.247663	40.761742	-7.295	18.472	2.057	1.297	B	40-2678	IIIR-31	—	—
427269	11.116948	41.917397	-7.269	17.201	2.043	0.000	B	—	—	—	—
33436	9.391909	40.403561	-7.248	18.012	2.273	0.790	A	—	—	—	R1
216250	10.252391	41.155861	-7.247	18.223	1.806	1.000	A	—	—	—	—
439882	12.023583	42.026192	-7.213	18.017	2.144	0.760	B	—	—	—	—
346421	11.278433	41.568855	-7.199	17.720	1.840	0.449	B	41-3637	R-81b	—	—
338914	10.559035	41.546288	-7.184	19.260	1.979	1.974	A	—	—	—	—
463349	11.718462	42.250755	-7.144	18.490	2.415	1.164	B	—	—	—	—
136803	10.543445	40.924122	-7.141	19.452	1.836	1.910	Q	40-3947	—	—	—
102137	10.196411	40.745743	-7.039	18.970	2.006	1.331	Q	40-2401	IIIR-30	—	—
8380	9.705883	40.199226	-6.986	18.865	2.349	1.381	A	—	—	—	—
95473	10.128913	40.719624	-6.973	18.943	1.912	1.446	A	40-1980	—	M0*	—
229986	10.941835	41.194000	-6.888	19.466	2.083	1.662	Q	40-4653	—	—	—
358614	11.341266	41.599960	-6.875	18.422	2.255	0.827	B	—	—	—	—
204943	10.787182	41.125546	-6.848	18.061	2.608	0.439	B	40-4392	R-131	—	—
82288	9.975927	40.667858	-6.826	19.938	1.965	2.089	Q	—	—	—	—
385173	11.519415	41.689789	-6.825	17.761	2.013	0.116	B	41-4616	—	—	—
286440	10.409627	41.388996	-6.825	18.002	2.017	0.357	B	41-0246	R-171	M0	—
139447	10.626180	40.940041	-6.817	19.897	1.897	2.030	Q	—	—	—	—
27200	9.838799	40.358631	-6.811	18.986	2.018	1.327	B	40-0528	IIIR-99	—	R8
411624	11.002398	41.827980	-6.811	18.357	1.878	0.698	A	41-2045	R-40	—	—
463820	11.352789	42.255173	-6.790	18.579	1.980	0.899	B	—	—	—	—
458999	11.381101	42.214844	-6.784	18.999	1.811	1.313	B	—	—	—	—
285099	11.122199	41.385464	-6.774	19.281	2.259	1.357	Q	41-2658	R-110	—	—
13787	10.081344	40.256355	-6.765	19.296	1.980	1.591	B	39-1144	—	—	—
380803	11.321597	41.663338	-6.763	19.215	1.959	1.270	Q	41-3867	—	M2.5*	—
153888	10.411914	40.999454	-6.749	18.345	2.182	0.624	B	40-3506	—	—	—
459075	11.381123	42.215511	-6.733	19.050	1.821	1.313	B	41-4128	—	—	—
249017	10.446620	41.260513	-6.728	19.772	2.237	1.807	Q	—	—	—	—
223296	10.506104	41.171646	-6.706	18.747	1.941	0.762	Q	—	—	—	—
77174	10.644314	40.642048	-6.689	19.392	1.953	1.611	B	—	—	—	—
306484	10.724109	41.455193	-6.620	18.509	1.961	0.659	A	—	—	—	—
211171	10.330422	41.143433	-6.615	19.479	2.194	1.405	Q	—	—	—	—
99820	10.678908	40.737354	-6.575	18.830	2.343	0.935	B	40-4234	—	—	—
916	9.840187	40.074886	-6.574	18.965	2.519	1.069	B	39-0926	—	—	—
206402	10.264723	41.130531	-6.564	19.836	1.900	1.711	Q	—	—	—	—
457329	11.344069	42.196171	-6.536	19.203	1.914	1.269	B	41-3973	—	—	—
154736	10.651431	41.001438	-6.531	18.642	1.883	0.703	A	40-4186	—	—	—
334859	10.554651	41.534081	-6.516	19.928	1.821	1.974	B	—	—	—	—
332378	11.152265	41.527172	-6.513	18.496	2.510	0.539	B	—	—	—	—
263242	11.065625	41.297363	-6.506	19.458	2.329	1.270	Q	—	—	—	—
234927	10.979662	41.218048	-6.491	18.067	2.204	0.088	A	40-4707	—	—	—
228566	10.824341	41.187141	-6.485	19.153	1.900	0.947	Q	—	—	—	—
232974	10.409659	41.208912	-6.480	18.016	2.409	0.000	Q	—	—	—	—
293476	11.126873	41.409916	-6.471	19.482	2.183	1.255	Q	—	R-105	—	—
105041	10.145855	40.756027	-6.461	19.260	2.251	1.251	A	—	—	—	—
26754	10.227870	40.355621	-6.450	19.694	2.160	1.674	B	40-2564	—	—	—
209898	10.286233	41.140270	-6.448	18.022	2.434	0.000	A	—	—	—	—
112591	9.934171	40.794487	-6.428	19.733	2.015	1.691	B	40-0914	—	—	—
475471	11.534462	42.385521	-6.424	19.905	1.974	1.859	B	—	—	—	—
150939	10.640384	40.992729	-6.416	18.302	2.074	0.248	A	40-4159	—	—	—
384965	11.306774	41.688457	-6.392	18.579	2.223	0.501	B	41-3786	—	—	—

Continued on next page

Table 4 – *Continued from previous page*

Nr. in MLV	Coordinates 2000.0		M_V	V	$(V-I)_0$	A_V	E	B88	H88	Sp	N89
17645	9.680671	40.292290	-6.390	19.091	2.133	1.011	B	40-0114	—	—	—
405303	10.993254	41.800545	-6.378	18.780	1.829	0.688	A	41-2011	R-42	—	—
285052	11.028757	41.385342	-6.347	18.859	1.811	0.736	B	41-2160	—	—	—
232548	10.820907	41.206753	-6.309	18.841	1.840	0.458	Q	—	—	—	—
299880	10.931031	41.431850	-6.290	18.758	1.882	0.577	B	—	—	—	—